



Upscaling of CO₂ vertical migration through a periodic layered porous medium: The capillary-free and capillary-dominant cases

Emmanuel Mouche*, Mohamed Hayek, Claude Mügler

Laboratoire des Sciences du Climat et de l'Environnement, UMR CEA-CNRS-UVSQ, Centre d'Etudes de Saclay, Orme des Merisiers, F-91191 Gif-sur-Yvette Cedex, France

ARTICLE INFO

Article history:

Received 11 February 2010

Received in revised form 15 July 2010

Accepted 16 July 2010

Available online 24 July 2010

Keywords:

Geological CO₂ sequestration

Two-phase flow

Buoyancy

Capillarity

Heterogeneity

Upscaling

ABSTRACT

We present an upscaled model for the vertical migration of a CO₂ plume through a vertical column filled with a periodic layered porous medium. This model may describe the vertical migration of a CO₂ plume in a perfectly layered horizontal aquifer. Capillarity and buoyancy are taken into account and semi-explicit upscaled flux functions are proposed in the two following cases: (i) capillarity is the main driving force and (ii) buoyancy is the only driving force. In both cases, we show that the upscaled buoyant flux is a bell-shaped function of the saturation, as in the case of a homogeneous porous medium. In the capillary-dominant case, we show that the upscaled buoyant flux is the harmonic mean of the buoyant fluxes in each layer. The upscaled saturation is governed by the continuity of the capillary pressure at the interface between layers. In the capillary-free case, the upscaled buoyant flux and upscaled saturation are determined by the flux continuity condition at the interface. As the flux is not continuous over the entire range of saturation, the upscaled saturation is only defined where continuity is verified, *i.e.* in two saturation domains. As a consequence, the upscaled buoyant flux is described by a piecewise continuous function. Two analytical approximations of this flux are proposed and this capillary-free upscaled model is validated for two cases of heterogeneity. Upscaled and cell averaged saturations are in good agreement. Furthermore, the proposed analytical upscaled fluxes provide satisfactory approximations as long as the saturation set at the inlet of the column is in a range where analytical and numerical upscaled fluxes are close.

© 2010 Elsevier Ltd. All rights reserved.

1. Introduction

Potential geological storage sites for the sequestration of carbon dioxide (CO₂), like deep saline aquifers or gas and oil reservoirs, are heterogeneous [8]. Two types of heterogeneity can be considered [4]: sedimentary heterogeneity and structural heterogeneity due to faults or fractures. These two types are classically described as a spatial hierarchy of architectures. Ringrose et al. [31], distinguish the lithofacies scale (10⁻²–10⁰ m), the geological scale (10⁰–10² m) and the reservoir scale. Structural heterogeneities are typically incorporated in the models at the reservoir scale. We consider here sedimentary heterogeneity at the lithofacies and geological scales only. They describe respectively recognizable association of lamina and laminasets and the spatial arrangement of lithofacies or rock units [31]. Indeed, this nested hierarchy controls phase flow parameters such as porosity, absolute permeability, relative-permeability and capillary pressure curves.

Numerical models have been developed and applied to synthetic or natural storage sites to assess the impact of the spatial variability of these parameters [14–16,22]. For memory and computational time

reasons, these reservoir models cannot account for the multi-scale variability, *i.e.* from the lamina-scale to the stratigraphic unit scale [27,31]. Because of their complexity they also cannot be used for site performance and risk assessment studies.

As reservoir models in petroleum engineering full-scale models of CO₂ storage sites need to be upscaled. Much of the upscaling approaches and techniques developed in reservoir modeling [1,10,11,31] can be used for this purpose. Nevertheless, gravity is often neglected, at least in oil water systems, and viscous forces are considered to be dominant at the reservoir scale [1]. Injected as a supercritical fluid, CO₂ is buoyant with respect to the site porewater; therefore gravity plays an important role in CO₂ injection and migration [8].

CO₂ sequestration in deep saline aquifers, such as the Utsira aquifer at the Sleipner site [37], is an option studied by many countries. Indeed, these geological formations offer the advantages of having more volume capacity than other types of formation and being the more abundant in the subsurface. Seismic profiles have tracked since the beginning of the injection in 1996 the CO₂ plume migration in Utsira sands [2]. They show that the plume rises buoyantly in the aquifer, ponds beneath low-permeability shale layers, and migrates progressively upwards through leaks in these layers. In many modeling studies Utsira is idealized as a 200 m thick stratified aquifer composed of high-permeability sand layers ($\approx 10^{-12}$ m²) separated

* Corresponding author. Tel.: +33 1 69 08 22 54.

E-mail addresses: emmanuel.mouche@cea.fr (E. Mouche), mohamed.hayek@gmail.com (M. Hayek), claudio.mugler@lscce.ipsl.fr (C. Mügler).

periodically by four to nine low-permeability shale layers [5,20]. These shale layers are considered either as continuous, but with microfractures represented by a homogenized absolute permeability of 10^{-14} m², or discontinuous and impermeable. In the first case, *i.e.* continuous layers, the plume is driven through the different layers mainly by capillarity and buoyancy and, far from the injection point, *i.e.* above the first lowest shale layer, the plume migration can be modeled as a one-dimensional vertical process. In the second case, *i.e.* discontinuous layers, the CO₂ plume is essentially buoyancy-driven and migrates through tortuous high-permeability pathways. Indeed the migration process is, in this last case, fully multi-dimensional. Recently Hesse and Woods [19] showed that the flux partitioning through a two dimensional periodic system of discontinuous impermeable barriers may be modeled as a dispersion process and, Green and Ennis-King [17] studied the statistics of high-permeability pathways in the case of a two dimensional random system. Other authors have modeled CO₂ migration as gravity currents [7] and, for instance, Neufeld and Huppert [25] developed such a model for Utsira assuming that CO₂ migration through continuous shale layers may be represented as a drainage process.

Nothing is known on the plume migration at a smaller scale, namely in the high-permeability layers. Saadtpoor et al. [32] analyzed the two dimensional migration of a CO₂ plume in geostatistical realizations of permeability distributed log-normally. The horizontal correlation length was equal to 1.5 m or 15.0 m and the vertical direction was assumed uncorrelated. They showed that, when capillarity is neglected, the plume migrates along tortuous vertical pathways of less hydraulic resistance, determined by the spatial correlation of permeability, and when capillarity is taken into account, and scaled to the permeability, the plume migrates along pathways of low capillary entry pressure. Introduction of this capillary heterogeneity leads to a new trapping mechanism that the authors call capillary trapping.

All these works show that CO₂ migration in a two- or three-dimensional heterogeneous aquifer is a complex process and the upscaling of this problem, recognized as an important issue for carbon sequestration, has not been tackled for the moment in the literature. In this paper, we consider the problem for a one-dimensional geometry: a vertical column filled with a periodic layered porous medium. As discussed previously, this uni-dimensional representation of a perfectly layered aquifer may be relevant for site modeling, and particularly in risk assessment models. More importantly it provides a basis for generalizations to higher dimensions.

To the authors knowledge, the upscaling of two-phase flow driven by injection, capillarity and gravity through a vertical periodic layered porous column has never been published, neither in the case where the injected phase is light (CO₂) nor in the case where it is dense, like dense nonaqueous phase liquids (DNAPL).

Van Duijn et al. [40] studied the injection of oil into a horizontal column filled initially with water. In this case, gravity is absent and capillarity is the only driving force. They considered a capillary pressure described by the Leverett model with a non zero entry pressure [38,39]. The objective was to derive and validate with numerical simulations an effective saturation transport equation which accounts for capillary oil trapping at the microscale, or lamina-scale, during water-drive in an oil reservoir. This trapping mechanism comes from the entry pressure discontinuity at the interface between a high and a low-permeability layer which induces an oil saturation discontinuity. To derive the effective saturation transport equation, van Duijn et al. followed the homogenization procedure introduced initially by Bensoussan et al. [6] or Sanchez Palencia [33] for periodic structures and applied to multiphase flow problems in periodic porous media by many authors such as Amaziane et al. [3] or Panfilov and Floriat [26] for two-phase flow in oil reservoirs, and Lewandowska et al. [23] for the upscaling of unsaturated flow. Later on, van Duijn et al. improved their upscaled model by considering higher

order terms in the asymptotic expansion of the capillary pressure continuity condition at the layer interface [41].

Quintard and Whitaker [29] studied also the case of a horizontal column with their original volume averaging technique based on scale separation [28]. They neglected dynamic effects associated with flow and transient effects and considered a capillary pressure curve with zero entry pressure. They proposed an effective saturation transport equation and effective relative-permeability and capillary pressure curves. Then, they discussed by means of numerical simulations how, far from the injection point, their upscaling approach can reproduce the space averaged saturation. Dale et al. [13] proposed effective curves in the steady state, based on an analytical solution of the steady-state saturation equation. The applicability of these parameters was evaluated by means of numerical simulations. In particular, they showed that their upscaled curves recover the capillary equilibrium condition when the injection rate tends to zero, and inversely the viscously dominated flow limit when the rate tends to infinity.

When gravity is added, *i.e.* the column is vertical and filled with a light phase (CO₂) and a dense phase (water), upscaling is expected to become a more complex task, essentially because the two-phase flow at the interface between two layers is complex and may follow different flow regimes [35]. Indeed, as the gravity (buoyant) flux depends on the absolute permeability and is a bell-shaped function of the saturation, it cannot be continuous at the layer interface over the entire range of saturation and, moreover, saturation is discontinuous in the range of flux where continuity is respected [18,34]. When capillarity is neglected, this leads to a CO₂ plume dynamics described as a succession of shocks and rarefaction waves. See Hayek et al. [16] for a description of the problem in 1D and 2D with an injection point at the bottom of the domain. Therefore consideration of capillarity and buoyancy leads to a general problem where both the total flux – equal to the sum of the viscous, buoyant and capillary fluxes – and the capillary pressure must be continuous at each interface. This imposes discontinuities of both saturation and saturation gradients at the interfaces. To the authors knowledge, Siddiqui and Lake [35] are the only authors who studied this issue for the analysis of secondary migration of hydrocarbon, *i.e.* from the reservoir into a seal, in the petroleum engineering context.

In this paper, we propose an upscaled model for the buoyant migration of a CO₂ plume in a vertical column filled with a periodically layered porous medium. Buoyancy and capillarity are considered, but injection is neglected. Following the work of van Duijn et al., we adopt the homogenization technique for periodic media of Bensoussan et al. [6]. We consider two cases: one, where capillarity is dominant and the other with no capillarity. This last case is often called the Buckley–Leverett problem with gravity [18]. The case where buoyancy and capillarity are of the same order of magnitude in a layer is much more complex and will be studied in a forthcoming paper. We show that in the first case, the upscaled CO₂ saturation transport equation is a nonlinear convection–diffusion type equation and, in the second one, a non linear convection type equation. In each case, upscaled flux functions must be determined numerically but in the second case, we propose two analytical approximations. Finally, the validity of the capillary-free upscaled model is studied by means of numerical experiments and the saturations obtained with numerical and analytical flux functions are compared and discussed.

2. The model

We consider a 1D-vertical column filled with a periodic layered porous medium made up of low and high-permeability layers (Fig. 1). Without any loss of generality, we assume that the layers have the same constant porosity, ϕ , and the same thickness equal to δ . The absolute permeabilities of the low and high-permeability layers are k_- and k_+ , respectively. The column length is H and supposed to be

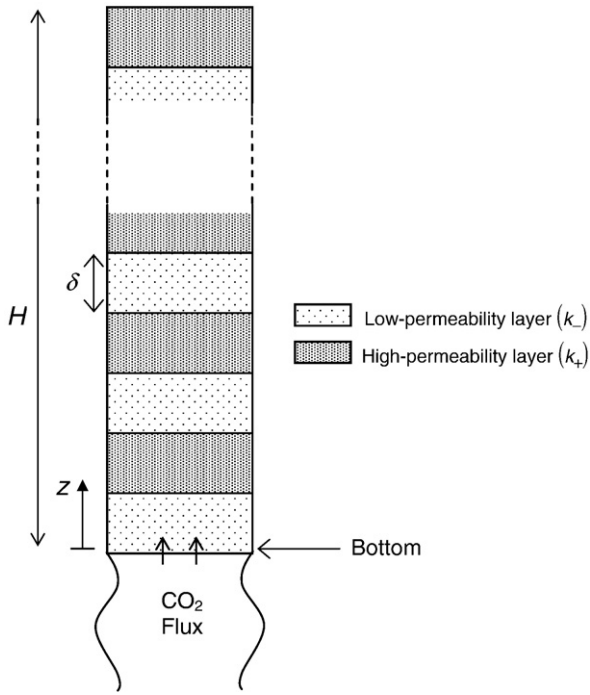


Fig. 1. Vertical column with high and low-permeability layers.

much greater than δ , and consequently the small parameter $\varepsilon = \delta/H$ is much smaller than one, $\varepsilon \ll 1$.

The flow of two immiscible and incompressible phases, water and CO₂, in the 1D-column is described by the mass balance equations:

$$\phi \frac{\partial S_\alpha}{\partial t} + \frac{\partial u_\alpha}{\partial z} = 0 \quad (1)$$

and by the modified Darcy's laws:

$$u_\alpha = -\frac{k(z)k_{r\alpha}(S_\alpha)}{\mu_\alpha} \left(\frac{\partial p_\alpha}{\partial z} - \rho_\alpha g \right) \quad (2)$$

where $\alpha = g$ for CO₂, called gas phase, and $\alpha = w$ for water, called liquid phase. Here S_α , u_α , p_α , $k_{r\alpha}$, μ_α , and ρ_α are the saturation, Darcy velocity, pressure, relative-permeability, viscosity, and density of phase α , respectively. g is the acceleration due to gravity, ϕ the porosity and the absolute permeability $k(z)$ is equal to either k_- or k_+ .

The most used relative-permeability models for CO₂ migration in geological media are the Brooks-Corey [9] and van Genuchten models [42]. In the present paper, the Brooks-Corey formula for relative-permeability is used

$$k_{rw}(S_g) = (1 - S_{eg})^{\frac{2+3\lambda}{\lambda}} \quad (3)$$

$$k_{rg}(S_g) = S_{eg}^2 \left[1 - (1 - S_{eg})^{\frac{2+\lambda}{\lambda}} \right]$$

where λ is the pore size distribution index. In Eq. (3), S_{eg} is the effective gas phase saturation given by:

$$S_{eg} = \frac{S_g - S_{rg}}{1 - S_{rg} - S_{rw}} \quad (4)$$

where $S_{r\alpha}$ ($\alpha = g, w$) is the residual saturation of phase α .

The phase saturations are constrained by:

$$S_w + S_g = 1. \quad (5)$$

This constraint and Eq. (1) yield to the total velocity

$$u_g + u_w = u(t) \quad (6)$$

which must be constant in space but may vary with time.

Capillary pressure is defined as

$$p_c(S_g, z) = p_g - p_w \quad (7)$$

and is given by the Leverett relationship [24]

$$p_c(S_g, z) = \sigma \sqrt{\frac{\phi}{k(z)}} J(S_g) \quad (8)$$

where σ is the interfacial tension between water and CO₂ and, J is the Leverett function. The porosity ϕ is assumed to be constant in the column. Here again, Brooks-Corey or van Genuchten models may be used for the J function. Only Brooks-Corey is considered here:

$$J(S_g) = (1 - S_{eg})^{-1/\lambda} \quad (9)$$

The entry pressure is defined as:

$$p_c(0, z) = \sigma \sqrt{\frac{\phi}{k(z)}} \quad (10)$$

This pressure is the minimum pressure that CO₂ must exert on water before it can enter into a fully water saturated column. Index g is now omitted and $S \equiv S_g$.

Eqs. (2), (6) and (7) lead to CO₂ Darcy velocity

$$u_g = \frac{u(t)}{k_{rw}(S)} f(S) + \frac{1}{\mu_w} k(z) f(S) \left((\rho_w - \rho_g) g - \frac{\partial p_c}{\partial z} \right) \quad (11)$$

where

$$f(S) = \frac{k_{rg}(S)k_{rw}(S)}{k_{rg}(S) + M k_{rw}(S)} \quad (12)$$

with $M = \mu_g/\mu_w$, the viscosity ratio. The three terms in Eq. (11) correspond to the contributions of, respectively, injection, buoyancy and capillarity to the CO₂ flux. One should notice that buoyancy is described by a bell-shaped function, $f(S)$, whereas injection is described by a "S"-shaped function, $f(S)/k_{rw}(S)$, usually called fractional flow function of the wetting phase. This difference of shape has a fundamental impact on the CO₂ plume dynamics [18]. In this paper, we assume that the flow is countercurrent, $u(t) = 0$, which means that there is no phase injection in the column. The flow of the gas and water phases is only driven by buoyancy and capillarity forces: due to density contrast, CO₂ is moving upwards and water downwards. The case $u(t) \neq 0$ will be briefly discussed in Section 3.

Substitution of Eq. (11) into Eq. (5) yields to the non linear advection-diffusion transport equation:

$$\phi \frac{\partial S}{\partial t} + \frac{\partial}{\partial z} \left(\frac{1}{\mu_w} k(z) f(S) \left((\rho_w - \rho_g) g - \frac{\partial p_c}{\partial z} \right) \right) = 0. \quad (13)$$

This equation has been studied, from a physical and/or numerical point of view, by different authors, mainly in the homogeneous porous medium case. Among them, we can cite Cunha et al. [12] who performed a laboratory experiment to analyze the motion of gas (atmospheric air) and liquid in a vertical column and used a numerical

scheme of Godunov type to model the experiment. More recently, Sillin et al. [36] analyzed the vertical motion of a gas plume by means of travelling-wave solutions and proposed their method to study CO₂ leaks from deep geological formations. It is important to emphasize that the bell shape of the flux function leads to a gas plume migration described as a sequence of shock and rarefaction waves at the top and the bottom of the plume. This sequence depends strongly on the relative-permeability relationships and on the initial plume saturation distribution.

As discussed in the introduction, very few works has been done on the heterogeneous porous medium case. To the authors knowledge, Siddiqui and Lake [35] are the only authors who addressed this issue. When capillarity is neglected, Eq. (13) reduces to the Buckley–Leverett equation with gravity. Among the few authors who studied this equation in heterogeneous porous media, we can cite, for instance, Kaasschieter [21] who studied extensively, from a mathematical point of view, the case of a permeability discontinuity. Recently Hayek et al. [18] analyzed the vertical motion of a CO₂ plume in a layered porous medium in 1D and in 2D. They proposed an explanation to the vertical CO₂ stratification observed at the Sleipner site [2].

Let us introduce the dimensionless variables $k = k / k_0$, $\hat{z} = z / H$ and $\hat{t} = \frac{t}{T(1-S_{rg}-S_{rw})}$ where H is a macroscopic length, the column height for instance, $T = H/u_{g0}$ is a characteristic travel time, with $u_{g0} = \frac{1}{\phi\mu_w} k_0 (\rho_w - \rho_g) g$, and k_0 is a characteristic absolute permeability. In what follows, to simplify the notation, we will note the dimensionless variables without hats, all the variables and unknowns having no dimension. These new variables bring Eq. (13) to the dimensionless form

$$\frac{\partial S}{\partial \hat{t}} + \frac{\partial}{\partial \hat{z}}(F(z, S)) = 0. \tag{14}$$

In Eq. (14), the dimensionless flux function $F(z, S)$ is given by:

$$F(z, S) = k(z)f(S) \left(1 - \frac{N_c}{\sqrt{k(z)}} J'(S) \frac{\partial S}{\partial z} \right) \tag{15}$$

where $J'(S) = \frac{dJ}{dS}$ and

$$N_c = \frac{\sigma}{(\rho_w - \rho_g)gH} \sqrt{\frac{\phi}{k_0}} \tag{16}$$

is called the capillary number. This dimensionless number, analogous to the reciprocal Bond number as pointed out by Silin et al. [36], measures the ratio between capillary and buoyancy forces. When $N_c = 0$ capillarity is neglected and Eq. (14) reduces to the Buckley–Leverett equation with gravity

$$\frac{\partial S}{\partial \hat{t}} + \frac{\partial}{\partial \hat{z}}(k(z)f(S)) = 0. \tag{17}$$

With the parameter values adopted by modelers for the simulation of CO₂ injection into the Utsira aquifer [5], one finds that N_c is of the order of 0.1 for a sand layer ($H \approx 25$ m, $k_0 \approx 3 \times 10^{-12}$ m² and $\phi \approx 45\%$) and greater than one for a shale layer ($H \approx 5$ m, $k_0 \approx 10^{-14}$ m² and $\phi \approx 10\%$).

From now, we will consider two models: the general model which takes into account buoyancy and capillarity and the capillary-free model where $N_c = 0$.

2.1. The model with capillarity and buoyancy

In this case, CO₂ saturation in a high-permeability layer is described by

$$\frac{\partial S}{\partial t} + \frac{\partial}{\partial z}(F_+) = 0 \tag{18}$$

where $F_+(S) = k_+f(S) \left(1 - \frac{N_{c-}}{\sqrt{k_+}} J'(S) \frac{\partial S}{\partial z} \right)$ is the associated flux. In the low-permeability layer:

$$\frac{\partial S}{\partial t} + \frac{\partial}{\partial z}(F_-) = 0 \tag{19}$$

where $F_-(S) = k_-f(S) \left(1 - \frac{N_{c-}}{\sqrt{k_-}} J'(S) \frac{\partial S}{\partial z} \right)$.

The continuity of the capillary pressure given by Eq. (8), at the interface between a high and a low-permeability layer implies that

$$\frac{J(S_{\text{int},-})}{\sqrt{k_-}} = \frac{J(S_{\text{int},+})}{\sqrt{k_+}} \tag{20}$$

where $S_{\text{int},+}$ and $S_{\text{int},-}$ are the saturation values on the high-permeability and low-permeability sides of the interface, respectively. As the entry pressure depends on the absolute permeability, this pressure is discontinuous at the interface and correlatively, the saturation at the interface is also discontinuous. Let us suppose that CO₂ is migrating from a high to a low-permeability layer, then the entry pressure discontinuity defines a threshold saturation S^* which satisfies:

$$\frac{J(S^*)}{\sqrt{k_+}} = \frac{J(0)}{\sqrt{k_-}}. \tag{21}$$

As long as $S_{\text{int},+} < S^*$, CO₂ pressure is below the entry pressure of the low-permeability layer and CO₂ cannot enter into the low-permeability layer; the interface is a zero flux boundary and $S_{\text{int},-} = 0$ and $S_{\text{int},+}$ increases with time. When $S_{\text{int},+} \geq S^*$, CO₂ pressure is greater or equal to the entry pressure of the low-permeability layer and CO₂ can enter into the low-permeability layer. Capillary pressure continuity is verified and saturations at the interface are ruled by Eq. (20). Moreover, flux must be continuous at the interface, therefore the saturations at the interface must also obey the relationship

$$F_+(S_{\text{int},+}) = F_-(S_{\text{int},-}). \tag{22}$$

2.2. The model without capillarity

When capillary effects are neglected, the CO₂ saturation in the column is described by the Buckley–Leverett equation with gravity given by Eq. (17). In a high-permeability layer, Eq. (14) reads

$$\frac{\partial S}{\partial t} + \frac{\partial}{\partial z}(F_+) = 0 \tag{23}$$

where $F_+(S) = k_+f(S)$ is the flux in the high-permeability layer. In the low-permeability layer:

$$\frac{\partial S}{\partial t} + \frac{\partial}{\partial z}(F_-) = 0 \tag{24}$$

where $F_-(S) = k_-f(S)$. The flux continuity at the interface between two layers implies

$$F_+(S_{\text{int},+}) = F_-(S_{\text{int},-}) \tag{25}$$

where $S_{\text{int},+}$ and $S_{\text{int},-}$ are the saturation values on each side of the interface. Indeed, as the global flux function $F(z, S) = k(z)f(S)$ depends on the absolute permeability, flux continuity at the interface leads to a saturation discontinuity [18].

3. The upscaled model

To upscale the model, we adopt the homogenization procedure introduced initially by Bensoussan et al. [6] or Sanchez Palencia [33] for periodic structures and applied to multiphase flow problems in periodic porous media by many authors [3,23,26]. More precisely, we follow in this work the modeling approach of van Duijn et al. [40,41] who studied the homogenization of two-phase flow with capillarity in a horizontal column and proposed an upscaled transport equation accounting for capillary trapping at the microscale.

In our problem, the small parameter is $\varepsilon = \delta/H$, the ratio of the layer thickness δ to the column height H . We first introduce two spatial variables, the macroscale variable z and the microscale variable $\zeta = z/\varepsilon$, which describe migration at the column scale and layer scale, respectively. Next, we expand asymptotically the saturation in powers of ε

$$S(z, t) \equiv S(z, \zeta, t) = S^0(z, \zeta, t) + \varepsilon S^1(z, \zeta, t) + \varepsilon^2 S^2(z, \zeta, t) + \dots \quad (26)$$

where the functions $S^i(z, \zeta, t)$ are periodic in ζ . The upscaled saturation, noted $\bar{S}(z, t)$, is defined as the integral of $S^0(z, \zeta, t)$ on a periodic cell:

$$\bar{S}(z, t) = \frac{1}{2} \int_{-1}^{+1} S^0(z, \zeta, t) d\zeta \quad (27)$$

where the cell contains a low-permeability and a high-permeability layer : for instance, $k = k_-$ for $-1 < \zeta < 0$ and $k = k_+$ for $0 < \zeta < 1$.

The derivation operator with respect to z is rewritten

$$\frac{\partial}{\partial z} \equiv \frac{\partial}{\partial z} + \frac{1}{\varepsilon} \frac{\partial}{\partial \zeta} \quad (28)$$

We substitute the expansion, Eq. (26), and the derivation operator, Eq. (28), into Eq. (14):

$$\frac{\partial(S^0 + \varepsilon S^1 + \dots)}{\partial t} + \left(\frac{\partial}{\partial z} + \frac{1}{\varepsilon} \frac{\partial}{\partial \zeta} \right) (F(\zeta, S)) = 0 \quad (29)$$

where the flux function, Eq. (15), is

$$F(\zeta, S) = A(\zeta, S) - B(\zeta, S) \left(\frac{\partial S}{\partial z} + \frac{1}{\varepsilon} \frac{\partial S}{\partial \zeta} \right) \quad (30)$$

with

$$\begin{aligned} A(\zeta, S) &= k(\zeta)f(S) \\ B(\zeta, S) &= N_c \sqrt{k(\zeta)} f(S) f'(S) \end{aligned} \quad (31)$$

The functions $f(S)$, $f'(S)$, $A(\zeta, S)$ and $B(\zeta, S)$ are expanded in powers of ε

$$\begin{aligned} f(S) &= f(S^0 + \varepsilon S^1 + \varepsilon^2 S^2 \dots) \\ &= f(S^0) + \varepsilon S^1 f'(S^0) + \varepsilon^2 \left(\frac{1}{2} (S^1)^2 f''(S^0) + S^2 f'(S^0) \right) + \dots \\ f'(S) &= f'(S^0) + \varepsilon S^1 f''(S^0) + \dots \\ A(\zeta, S) &= A(\zeta, S^0) + \varepsilon S^1 A'(\zeta, S^0) + \dots \\ B(\zeta, S) &= B(\zeta, S^0) + \varepsilon S^1 B'(\zeta, S^0) + \dots \end{aligned} \quad (32)$$

These expansions are inserted into the flux expression, Eq. (30), and the terms of the same power ε^n are brought together. This leads to the flux expansion

$$F(\zeta, S) = \varepsilon^{-1} F^{-1}(\zeta, S^0) + \varepsilon^0 F^0(\zeta, S^0, S^1) + \varepsilon^1 F^1(\zeta, S^0, S^1, S^2) + \dots \quad (33)$$

where

$$\begin{aligned} \varepsilon^{-1}: F^{-1}(\zeta, S^0) &= -B(\zeta, S^0) \frac{\partial S^0}{\partial \zeta} \\ \varepsilon^0: F^0(\zeta, S^0, S^1) &= A(\zeta, S^0) - B(\zeta, S^0) \left(\frac{\partial S^0}{\partial z} + \frac{\partial S^1}{\partial \zeta} \right) - S^1 B'(\zeta, S^0) \frac{\partial S^0}{\partial \zeta} \end{aligned} \quad (34)$$

Finally, we obtain the following saturation equations for the different orders

$$\begin{aligned} \varepsilon^{-2}: \frac{\partial F^{-1}}{\partial \zeta} &= -\frac{\partial}{\partial \zeta} \left(B(\zeta, S^0) \frac{\partial S^0}{\partial \zeta} \right) = 0 \\ \varepsilon^{-1}: \frac{\partial F^{-1}}{\partial z} + \frac{\partial F^0}{\partial \zeta} &= -\frac{\partial}{\partial z} \left(B(\zeta, S_0) \frac{\partial S^0}{\partial \zeta} \right) \\ &+ \frac{\partial}{\partial \zeta} \left(A(\zeta, S^0) - B(\zeta, S_0) \left(\frac{\partial S^0}{\partial z} + \frac{\partial S^1}{\partial \zeta} \right) - S^1 B'(\zeta, S_0) \frac{\partial S^0}{\partial \zeta} \right) = 0 \\ \varepsilon^0: \frac{\partial S^0}{\partial t} + \frac{\partial F^0}{\partial z} + \frac{\partial F^1}{\partial \zeta} &= 0. \end{aligned} \quad (35)$$

According to Section 2, if CO₂ is injected at the bottom of the column, the flow is no more countercurrent and the total velocity $u(t) \neq 0$ in Eq. (11). Therefore an additional scalar flux component which depends on saturation must be added to the buoyant component. Let us call this component $\alpha qu(S)$ where q is the injection rate, assumed to be constant with time, $u(S) = f(S)/k_{rg}(S)$ and α is a constant which depends on the problem parameters but not on permeability. We see that all the upscaling procedure remains unchanged when this component is added: the zeroth order flux reads $F^0(\zeta, S^0) = k(\zeta)f(S^0) + \alpha qu(S^0)$ and the upscaled variables and equations do not change. Nevertheless, the dimensionless variables may change as one may prefer to define a characteristic travel time governed by injection, $T = H/q$, rather than buoyancy as it is the case here.

As previously mentioned in Section 2.1, we consider two models: (i) a model which takes into account buoyancy and capillarity and, (ii) a capillary-free model with $N_c = 0$. Moreover, we assume that in the first case, capillarity is dominant, that is $N_c \geq 1$. As a matter of fact, in this case, the lowest order in ε of the flux expansion, Eq. (33), represents capillary diffusion in a layer; this case is called the capillary limit by van Duijn et al. [40]. When $N_c \approx \varepsilon$, case called balance case by the same authors, it is easy to see from the previous expansions in powers of ε that the flux expansion is $F(\zeta, S) = \varepsilon^0 F^0(\zeta, S^0) + \dots$ where $F^0(\zeta, S^0, S^1) = A(\zeta, S^0) - B(\zeta, S^0) \frac{\partial S^0}{\partial \zeta}$ which describes capillary diffusion and buoyancy in a layer. This case is much more complex to analyze than the capillary-dominant case and is not studied in this paper.

3.1. The capillary-dominant model

The ε^{-2} order of the saturation equation, Eq. (35), shows that the ε^{-1} order of the flux, given by Eq. (34) and equal to $F^{-1}(\zeta, S_0) = -B(\zeta, S^0) \frac{\partial S^0}{\partial \zeta}$, is constant in each layer of a cell and depends only on the macroscale variable z . Moreover, flux continuity at the interface between the two layers of a cell imposes that this flux, F^{-1} , is constant in a cell. Following van Duijn demonstration [40],

this constant flux condition and the periodicity of S^0 lead to the result $F^{-1} = 0$. Therefore S^0 is constant in each layer and we write $S^0 \equiv S^0_-(z, t)$ ($-1 < \zeta < 0$) and $S^0 \equiv S^0_+(z, t)$ ($0 < \zeta < 1$).

As for the ε^{-2} order, the ε^{-1} order of the saturation equation, Eq. (35), shows that the ε^0 order of the flux, noted F^0 in Eq. (34), is constant in each cell and depends only on the macroscale variable z . Coming back to the initial variables given by Eq. (31), we can write:

$$\begin{aligned} -1 < \zeta < 0: \quad F^0(z, t) &= k_- f(S^0_-) - N_c \sqrt{k_-} f(S^0_-) J'(S^0_-) \left(\frac{\partial S^0_-}{\partial z} + \frac{\partial S^0_-}{\partial \zeta} \right) \\ 0 < \zeta < 1: \quad F^0(z, t) &= k_+ f(S^0_+) - N_c \sqrt{k_+} f(S^0_+) J'(S^0_+) \left(\frac{\partial S^0_+}{\partial z} + \frac{\partial S^0_+}{\partial \zeta} \right) \end{aligned} \quad (36)$$

where $S^1 \equiv S^1_-(\zeta, z, t)$ for $-1 \leq \zeta \leq 0$ and $S^1 \equiv S^1_+(\zeta, z, t)$ for $0 \leq \zeta \leq 1$.

The saturation expansion, Eq. (26), is also inserted into the capillary pressure continuity relationship at the layers interface, Eq. (20):

$$\frac{J(S^0_- + \varepsilon S^1_-(0, z, t) + \dots)}{\sqrt{k_-}} = \frac{J(S^0_+ + \varepsilon S^1_+(0, z, t) + \dots)}{\sqrt{k_+}} \quad (37)$$

The J functions are expanded and the following relationships are obtained [33]:

$$\begin{aligned} \varepsilon^0: \quad \frac{J(S^0_-)}{\sqrt{k_-}} &= \frac{J(S^0_+)}{\sqrt{k_+}} \\ \varepsilon^1: \quad S^1_-(0, z, t) \frac{J'(S^0_-)}{\sqrt{k_-}} &= S^1_+(0, z, t) \frac{J'(S^0_+)}{\sqrt{k_+}} \end{aligned} \quad (38)$$

Periodicity and continuity of capillary pressure lead to another relationship linking the values of the ε order capillary pressure expansion at the two cell endpoints, $\zeta = \pm 1$, [41]:

$$S^1_-(-1, z, t) \frac{J'(S^0_-)}{\sqrt{k_-}} = S^1_+(+1, z, t) \frac{J'(S^0_+)}{\sqrt{k_+}} \quad (39)$$

With the help of Eqs. (38) and (39), saturation profiles S^1_- and S^1_+ and gradients $\frac{\partial S^1_-}{\partial \zeta}$ and $\frac{\partial S^1_+}{\partial \zeta}$ of Eq. (36) are found and the ε^0 order of the flux, defined as F^0 in Eq. (36), finally reads:

$$F^0(z, t) = \frac{2}{\frac{1}{k_- f(S^0_-)} + \frac{1}{k_+ f(S^0_+)}} \left(1 - \frac{N_c}{2} \left(\frac{J'(S^0_-)}{\sqrt{k_-}} \frac{\partial S^0_-}{\partial z} + \frac{J'(S^0_+)}{\sqrt{k_+}} \frac{\partial S^0_+}{\partial z} \right) \right) \quad (40)$$

The integration over a cell of the ε^0 order saturation equation, Eq. (35), leads to the following upscaled transport equation:

$$\frac{\partial \bar{S}}{\partial t} + \frac{\partial \bar{F}(\bar{S})}{\partial z} = 0 \quad (41)$$

where, due to the periodicity condition, the third term of the ε^0 equation, $\frac{\partial F^1}{\partial \zeta}$, is null after integration. The upscaled saturation, Eq. (27) is:

$$\bar{S}(z, t) = \frac{1}{2} (S^0_- + S^0_+) \quad (42)$$

and the upscaled flux function $\bar{F}(\bar{S}(z, t)) \equiv F^0(z, t)$ is defined as:

$$\begin{aligned} 0 \leq \bar{S} \leq \bar{S}^*: \quad \bar{F}(\bar{S}) &= 0 \\ \bar{S}^* \leq \bar{S} \leq 1: \quad \bar{F}(\bar{S}) &= \bar{G}(\bar{S}) \left(1 - N_c \frac{\partial \bar{P}_c(\bar{S})}{\partial z} \right) \end{aligned} \quad (43)$$

where $\bar{S}^* = S^* / 2$. The upscaled buoyant flux function is:

$$\bar{G}(\bar{S}) = \frac{2}{\frac{1}{k_- f(S^0_-)} + \frac{1}{k_+ f(S^0_+)}} \quad (44)$$

and the upscaled dimensionless capillary pressure:

$$\bar{P}_c(\bar{S}) = \frac{J(S^0_-)}{\sqrt{k_-}} = \frac{J(S^0_+)}{\sqrt{k_+}} \quad (45)$$

Following the definition of the threshold saturation S^* , Eq. (21), as long as $S^0_+ < S^*$, the CO₂ cannot enter into the low-permeability layer, then $S^0_- = 0$ ($\bar{S} < \bar{S}^* = S^* / 2$) and the flux $F^0 = 0$ ($\bar{F}(\bar{S}) = 0$). Finally, the upscaled equation, Eq. (41), may be rewritten as a non linear diffusion–advection transport equation

$$\frac{\partial \bar{S}}{\partial t} + \frac{\partial}{\partial z} \left(\bar{G}(\bar{S}) - \bar{D}(\bar{S}) \frac{\partial \bar{S}}{\partial z} \right) = 0 \quad (46)$$

where the upscaled diffusivity is

$$\bar{D}(\bar{S}) = \bar{G}(\bar{S}) \frac{dP_c(\bar{S})}{d\bar{S}} \quad (47)$$

The upscaled buoyant flux function $\bar{G}(\bar{S})$ can be interpreted as the harmonic cell average of the low and high-permeability layer buoyant flux functions, i.e. $k_+ f$ and $k_- f$. This is an expected result for a migration process perpendicular to the layering of a porous medium. Harmonic averaged functions have also been obtained by van Duijn et al. [41] for the horizontal column.

The functions $\bar{P}_c(\bar{S})$, $\bar{G}(\bar{S})$ and $\bar{D}(\bar{S})$ are plotted in Figs. 2 and 4 for two different permeability ratios: $k_-/k_+ = 0.3$ (Figs. 2a, 3a and 4a) and $k_-/k_+ = 0.05$ (Figs. 2b, 3b and 4b), with $k_+ = 1$. In these figures, the function $f(S)$ is normalized against its maximum value. The fluid properties and relative-permeability values are given in Table 1. The threshold saturation values are $S^* = 0.505$ ($\bar{S}^* = 0.2775$) and $S^* = 0.6675$ ($\bar{S}^* = 0.3587$) for $k_-/k_+ = 0.3$ and $k_-/k_+ = 0.05$, respectively (Fig. 2). We see that $\bar{G}(\bar{S})$ is a bell-shaped curve, as in the case of a homogeneous porous medium, but it is much more asymmetric in the layered case (see Fig. 5 which shows $k_+ f(S)$ and $k_- f(S)$ for $k_-/k_+ = 0.3$). The contributions of each layer to $\bar{G}(\bar{S})$, i.e. $2k_- f(S^0_-)$ and $2k_+ f(S^0_+)$ with $\bar{S} = (S^0_- + S^0_+) / 2$, are also plotted in Fig. 3. It shows that the vertical migration of the CO₂ plume is mainly controlled by the low-permeability layer in the ascending part of the curve, i.e. for \bar{S} close to \bar{S}^* , and by the high-permeability layer in the descending part. The maximum of $\bar{G}(\bar{S})$ for $k_-/k_+ = 0.05$ (Fig. 3b) is approximately three orders of magnitude lower than for $k_-/k_+ = 0.3$ (Fig. 3a). This ratio, which is lower than that of the low-permeability layer permeabilities for the two cases, i.e. $k_-/k_+ = 0.16$, is mainly explained

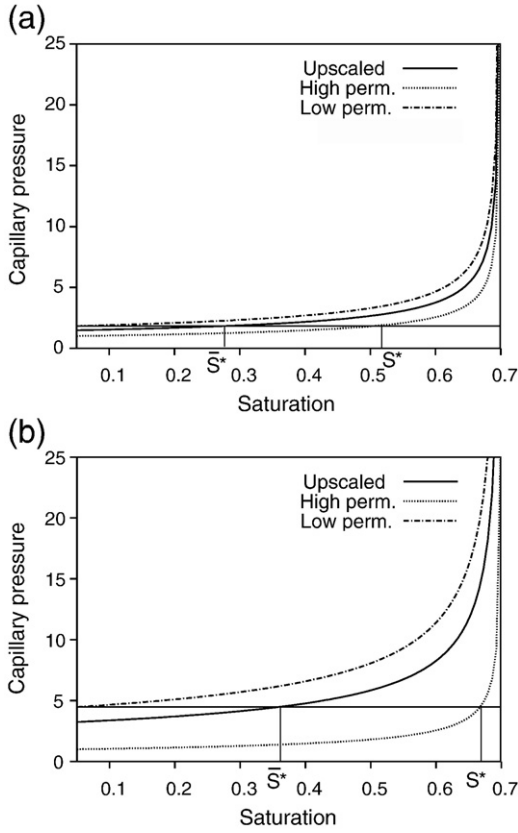


Fig. 2. Upscaled, low and high-permeability layer capillary pressure curves for (a) $k_-/k_+ = 0.3$ and for (b) $k_-/k_+ = 0.05$.

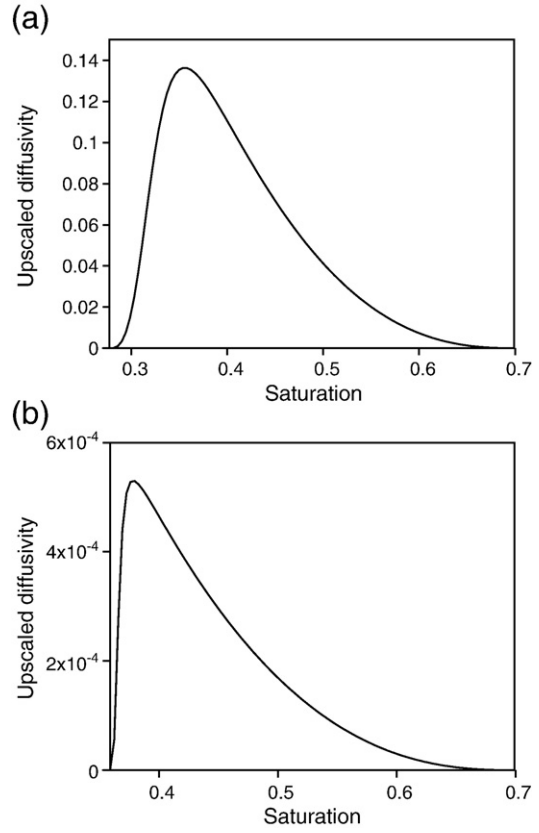


Fig. 4. Upscaled diffusivity $\bar{D}(\bar{S})$ for (a) $k_-/k_+ = 0.3$ and for (b) $k_-/k_+ = 0.05$.

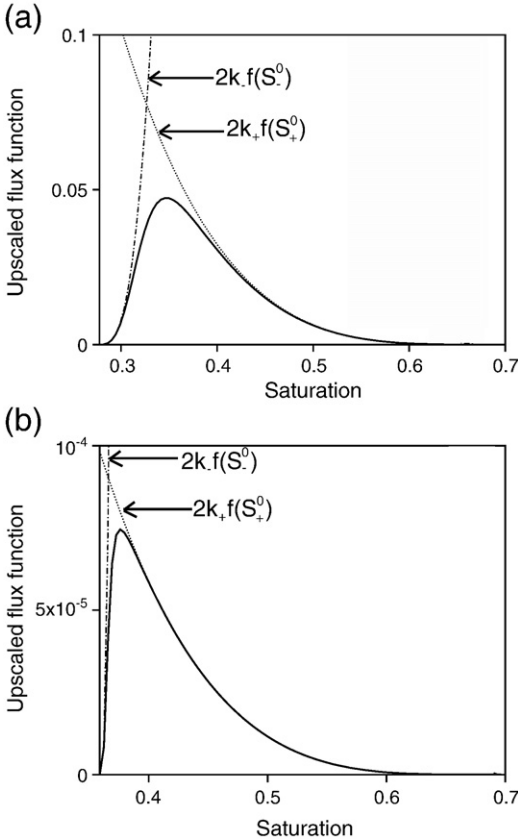


Fig. 3. Upscaled buoyant flux function $\bar{C}(\bar{S})$ and its two contributions $2k_-f(S^0_-)$ and $2k_+f(S^0_+)$ with $\bar{S} = (S^0_- + S^0_+)/2$ for (a) $k_-/k_+ = 0.3$ and for (b) $k_-/k_+ = 0.05$.

by the function $f(S^0_+ > S^*)$ which decreases rapidly when the threshold saturation value S^* increases, i.e. when k_- decreases (Fig. 2).

3.2. The capillary-free model

In this Section, we investigate the case $N_c = 0$. According to Eqs. (30) and (31) $B(\zeta, S) = 0$ and the flux is $F(\zeta, S) = A(\zeta, S) = k(\zeta)f(S)$. The flux expansion given in Eq. (33) reduces to $F(\zeta, S) = \varepsilon^0 F^0(\zeta, S^0) + \dots$ and the saturation equation for the different orders given by Eq. (35) becomes:

$$\begin{aligned} \varepsilon^{-1}: \quad \frac{\partial F^0(\zeta, S^0)}{\partial \zeta} &= \frac{\partial (k(\zeta)f(\zeta, S^0))}{\partial \zeta} = 0 \\ \varepsilon^0: \quad \frac{\partial S^0}{\partial t} + \frac{\partial F^0}{\partial z} + \frac{\partial F^1}{\partial \zeta} &= 0 \end{aligned} \tag{48}$$

The ε^{-1} order equation shows that the flux at the ε^0 order $F^0(\zeta, S^0) = k(\zeta)f(\zeta, S^0)$ is constant on a cell and depends only on the

Table 1
Fluids properties.

Parameters	Units	Values
Gas viscosity μ_g	$[\text{kg} \cdot \text{m}^{-1} \cdot \text{s}^{-1}]$	4.38×10^{-5}
Liquid viscosity μ_w	$[\text{kg} \cdot \text{m}^{-1} \cdot \text{s}^{-1}]$	0.25×10^{-3}
Residual saturation of gas phase S_{rg}	[-]	0.05
Residual saturation of liquid phase S_{rw}	[-]	0.3
Pore size distribution index λ	[-]	2

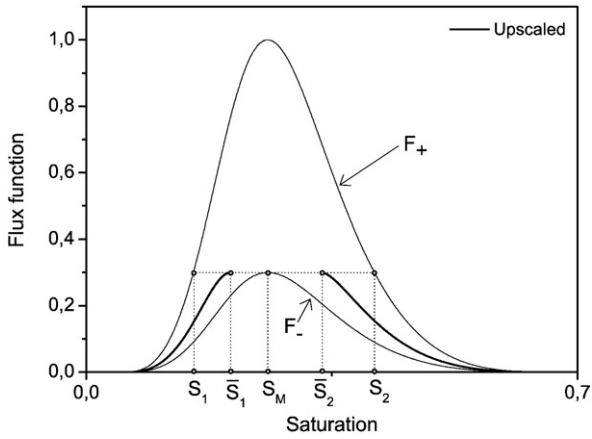


Fig. 5. Buoyant flux functions of the low and high-permeability layers, F_- and F_+ , respectively, and upscaled gravity flux function for $k_-/k_+ = 0.3$. Flux functions are normalized against the maximum of $f(S)$.

macroscale variable z . Therefore, saturation S^0 is constant in each layer and can be written as:

$$\begin{aligned} -1 < \zeta < 0: & F^0(z, t) = k_- f_-(S_-^0(z, t)) \\ 0 < \zeta < 1: & F^0(z, t) = k_+ f_+(S_+^0(z, t)) \end{aligned} \quad (49)$$

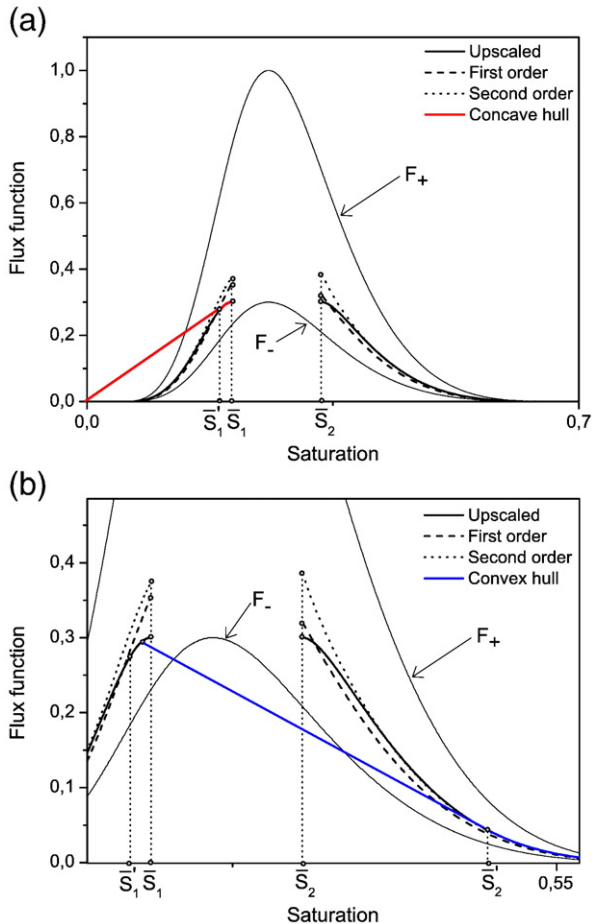


Fig. 6. Upscaled, first and second order buoyant flux functions, $k_-/k_+ = 0.3$. (a) convex hull and (b) concave hull.

where S_+^0 and S_-^0 are the saturation values in the high- and low-permeability layers, respectively. Integration of the ε^0 equation on a cell leads to the upscaled transport equation

$$\frac{\partial \bar{S}}{\partial t} + \frac{\partial \bar{F}(\bar{S})}{\partial z} = 0 \quad (50)$$

where, due to the periodicity condition, the third term of the ε^0 equation is null after integration. For a couple of saturations S_+^0 and S_-^0 satisfying the flux continuity condition given by Eq. (49), the upscaled saturation, is given by Eq. (42) and the upscaled flux function is $\bar{F}(\bar{S}(z, t)) \equiv F^0(z, t)$.

To determine the upscaled flux function, we assume that, first, S_+^0 and the associated flux $F^0 = k_+ f_+(S_+^0(z, t))$ are known, then the flux continuity condition, Eq. (49), is inverted to obtain the corresponding S_-^0 and finally the upscaled flux function is described by the couple (\bar{S}, F^0) .

As for the capillary-dominant model described in Section 3.1, two permeability ratios k_-/k_+ are considered: $k_-/k_+ = 0.3$ and $k_-/k_+ = 0.05$. The fluid properties and the relative-permeability values are given in Table 1. Hayek et al. [18] showed that flux continuity cannot be verified for the whole range of S_+^0 values but only on two segments: $0 \leq S_+^0 \leq S_1$ and $S_2 \leq S_+^0 \leq 1 - S_{rw}$. The two saturations S_1 and S_2 are given by the relationship:

$$F_+(S_1) = F_+(S_2) = F_-(S_M) \quad (51)$$

where S_M is the saturation at which function f is maximum and the flux functions are $F_- \equiv F^0 = k_- f_-(S_-)$ and $F_+ \equiv F^0 = k_+ f_+(S_+)$. Fig. 5 shows the flux continuity for the case $k_-/k_+ = 0.3$.

This constraint defines two ranges of upscaled saturation $0 \leq \bar{S} \leq \bar{S}_1$ and $\bar{S}_2 \leq \bar{S} \leq 1 - S_{rw}$ where $\bar{S}_1 = (S_1 + S_M) / 2$ and $\bar{S}_2 = (S_2 + S_M) / 2$ with $\bar{F}(\bar{S}_1) = \bar{F}(\bar{S}_2) = F_-(S_M)$. Therefore upscaled saturations lying between \bar{S}_1 and \bar{S}_2 do not exist (Fig. 5). This is a direct consequence of the non-monotonicity of the flux function (*i.e.* bell-shaped function). Indeed, if one thinks of a monotone flux function depending on absolute permeability, one can easily see that the upscaled flux function is a continuous monotone function defined in a single saturation domain. When the ratio $k_-/k_+ \rightarrow 0$ we have $\bar{S}_1 \rightarrow S_{rg}$ and $\bar{S}_2 \rightarrow (1 - S_{rw})$ and inversely when $k_-/k_+ \rightarrow 1$ we have \bar{S}_1 and $\bar{S}_2 \rightarrow S_M$.

The upscaled flux function must be computed numerically for each permeability ratio k_-/k_+ . Nevertheless an analytical approximation of this function can be proposed as follows. Let us write $S_-^0 = \bar{S} + \delta\bar{S}$ and $S_+^0 = \bar{S} - \delta\bar{S}$, then the flux continuity, Eq. (49), may be written $k_+ f(\bar{S} - \delta\bar{S}) = k_- f(\bar{S} + \delta\bar{S})$. Let us expand the f function up to the second order in $\delta\bar{S}$:

$$f(\bar{S} \pm \delta\bar{S}) \approx f(\bar{S}) \pm \delta\bar{S} f'(\bar{S}) + \frac{1}{2} \delta\bar{S}^2 f''(\bar{S}). \quad (52)$$

Eliminating $\delta\bar{S}$ leads to the upscaled flux function

$$\bar{F}(\bar{S}) = K(k_+, k_-) \frac{2(f'(\bar{S}))^2}{f''(\bar{S})} \left(1 - \sqrt{1 - \frac{2f(\bar{S})f''(\bar{S})}{(f'(\bar{S}))^2} (R(k_+, k_-))^2} \right) \quad (53)$$

where $K(k_+, k_-) = \frac{\sigma(k_+, k_-)}{(\delta(k_+, k_-))^2}$ and $R(k_+, k_-) = \frac{\delta(k_+, k_-)}{\sigma(k_+, k_-)}$ with $\delta(k_+, k_-) = \frac{1}{k_+} - \frac{1}{k_-}$ and $\sigma(k_+, k_-) = \frac{1}{k_+} + \frac{1}{k_-}$. We call Eq. (53) second order approximation.

If we neglect the second order derivative f'' , we obtain the first order approximation

$$\bar{F}(\bar{S}) = K_H(k_+, k_-) f(\bar{S}) \quad (54)$$

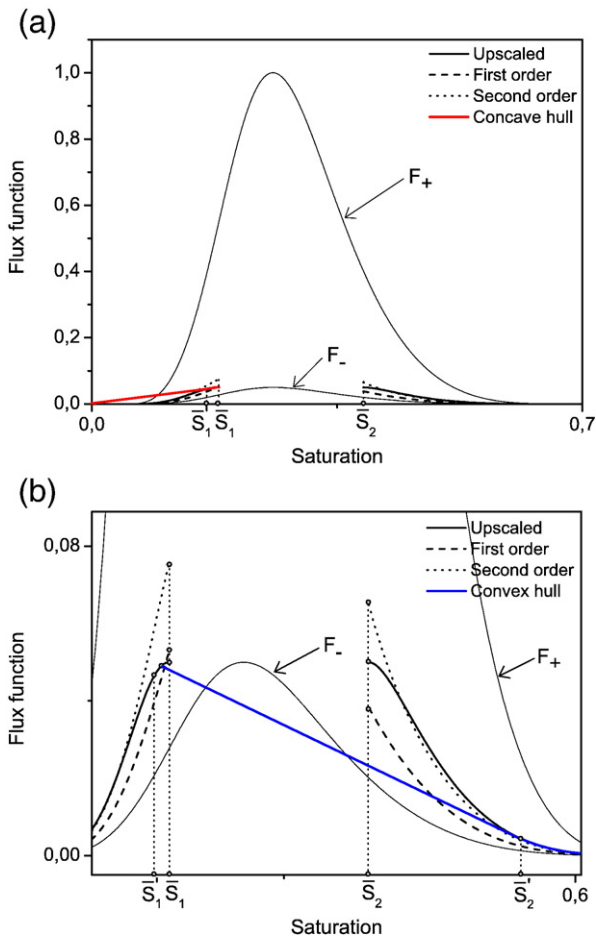


Fig. 7. Upscaled, first and second order buoyant flux functions for $k_-/k_+ = 0.05$. (a) convex hull and (b) concave hull.

where $K_H(k_+, k_-) = 2/\sigma(k_+, k_-)$ is the harmonic mean of the permeabilities of the low and high-permeability layers. It should be noticed that in this last approximation, the dependency of the upscaled flux on the upscaled saturation is not affected by upscaling, which is not the case in the second order approximation. A harmonic mean as an effective permeability is not a surprising result for a transport process normal to the layering [30].

The upscaled fluxes computed numerically and obtained from the first and second order approximations are plotted in Figs. 6 and 7 for $k_-/k_+ = 0.3$ and $k_-/k_+ = 0.05$, respectively. In these figures, the flux functions are normalized against the maximum of $f(S)$. As expected the second order gives a better approximation of the upscaled flux for saturations not too close to \bar{S}_1 and \bar{S}_2 , and is above the exact flux, particularly in the neighbourhood of \bar{S}_1 and \bar{S}_2 . Inversely the first order is below the exact flux function. None of the approximations reconstitute the curvature of the upscaled flux in the neighbourhoods of \bar{S}_1 and \bar{S}_2 .

An interesting asymptotic case is $k_- \ll k_+$. In this case, we see that when $k_-/k_+ \rightarrow 0$ we have $\bar{S} \rightarrow S_0^0 / 2$ where $S_0^0 \rightarrow 0$, and the upscaled flux function $\bar{F}(\bar{S}) \rightarrow k_- f(2\bar{S})$.

Following the remark made at the end of Section 3 on injection, we see that if injection is taken into account, the upscaled flux function depends on the injection rate q . This dependence cannot be isolated explicitly in the upscaled flux under the form of an upscaled injection term like $\bar{\alpha} \bar{q} \bar{u}(\bar{S})$. An expansion of the flux in $\delta \bar{S}$ like in Eq. (52) leads to nonlinear and fractional terms with respect to the injection rate q , even in the first order approximation.

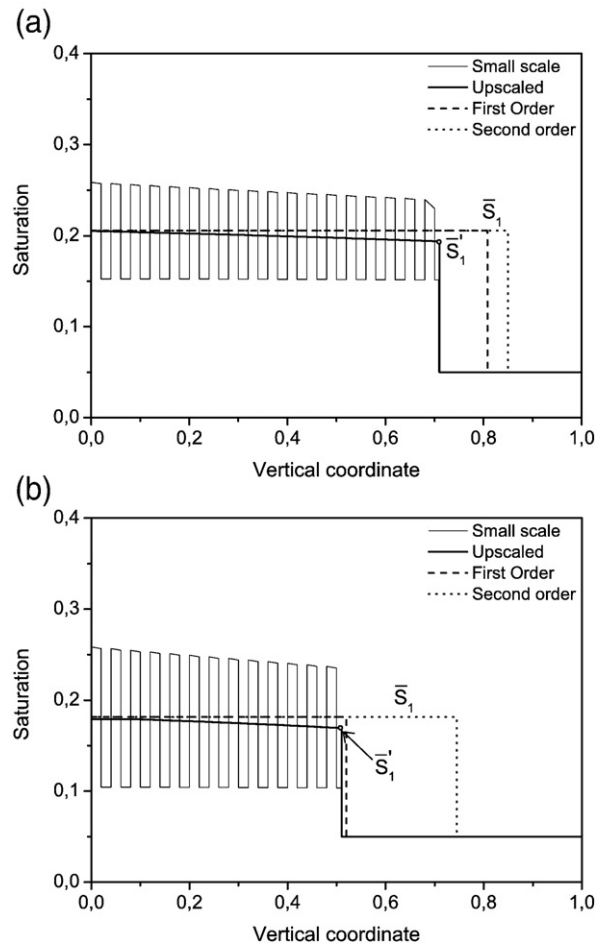


Fig. 8. Saturation distributions before the plume reaches the top of the column. Saturation at the bottom set to \bar{S}_1 . (a) $k_-/k_+ = 0.3$ and (b) $k_-/k_+ = 0.05$.

3.3. Validation of the upscaled capillary-free model

In this Section, we compare the upscaled model with the small-scale model in the capillary-free case. Three upscaled flux functions are considered: the exact flux function, obtained numerically, and the first order and second order approximations, discussed previously that we call first order flux function and second order flux function. All the models are solved analytically and the solutions are exact [16]. Two permeability ratios k_-/k_+ are studied, 0.05 and 0.3, and the small parameter ε , ratio of the layer thickness to the column height is set to 1/50. CO₂ saturation is imposed at the bottom of the column at $z = 0$, although the top of the column at $z = 1$ is a zero flux boundary.

The saturation profiles obtained before and after the CO₂ plume have reached the top of the column are displayed in Figs. 8 and 9. Figs. 8a and 9a, and 8b and 9b correspond to the cases $k_-/k_+ = 0.3$ and $k_-/k_+ = 0.05$, respectively. CO₂ saturation at the bottom of the column is set to \bar{S}_1 , where $\bar{S}_1 = 0.21$ for $k_-/k_+ = 0.3$ and $\bar{S}_1 = 0.18$ for $k_-/k_+ = 0.05$. The piecewise periodic shape of the small-scale saturation distributions has been discussed in [18]. The exact upscaled saturation distributions fit perfectly well with the cell averaged solution. These two distributions are described by a shock between $\bar{S} = 0$ and $\bar{S} = \bar{S}_1$ and a rarefaction wave between $\bar{S} = \bar{S}_1$ and $\bar{S} = \bar{S}_1'$, where \bar{S}_1' is shown in Figs. 6 and 7. These saturations describe the convex hull of the low saturation branch of the exact upscaled flux function (Figs. 6a and 7a). The saturation distributions computed with the first and second order fluxes, called first and second order saturation distributions, are described by shocks only and they travel

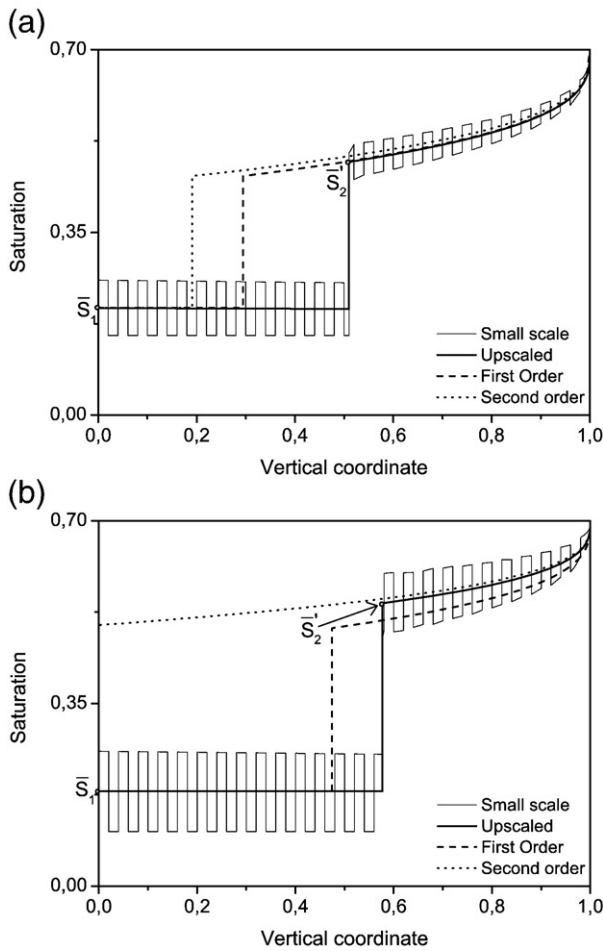


Fig. 9. Saturation distributions after the plume has reached the top of the column. Saturation at the bottom set to \bar{S}_1 . (a) $k_-/k_+ = 0.3$ and (b) $k_-/k_+ = 0.05$.

faster than the “exact” shock, and the “second order” shock travels faster than the “first order” shock, particularly in the case $k_-/k_+ = 0.05$. This is explained in Figs. 6a and 7a which show that: i) the convex hull of the low saturation branch of the exact flux function is made up of a straight line between $\bar{S} = 0$ and $\bar{S} = \bar{S}_1$ and by the flux function between $\bar{S} = \bar{S}_1$ and $\bar{S} = \bar{S}_1$; ii) the convex hulls of the low saturation branches of the first and second order flux functions are straight lines between $\bar{S} = 0$ and $\bar{S} = \bar{S}_1$; iii) the slope of the straight line describing the “second order” convex hull is greater than that describing the “first order” convex hull, and this difference is more pronounced for $k_-/k_+ = 0.05$ than for $k_-/k_+ = 0.3$. Let us recall that the shock velocity is proportional to this slope.

Once the plume has reached the top of the column, CO_2 starts to accumulate below the top, as shown in Fig. 9. Again the exact upscaled distributions, computed with the exact upscaled flux function, fits perfectly well with the cell averaged solution. Now, the saturation distributions depend on both low- and high-saturation branches of the flux functions (Figs. 6 and 7). The distributions are described by a rarefaction wave between $\bar{S} = S_{rg}$, at the top of the column where the flux is zero, and $\bar{S} = \bar{S}_2$, and a reflected shock between $\bar{S} = \bar{S}_2$ and $\bar{S} = \bar{S}_1$ at the bottom of the column. These saturations describe the concave hull of the flux function between $\bar{S} = \bar{S}_1$ and $\bar{S} = S_{rg}$ (Figs. 6b and 7b). This concave hull is made up of the flux function between $\bar{S} = S_{rg}$ and $\bar{S} = \bar{S}_2$ and of the straight line between $\bar{S} = \bar{S}_2$ and $\bar{S} = \bar{S}_1$. To be more precise, one must say that the concave hull evolves slightly with time: the straight line is defined between $\bar{S}_{right} = \bar{S}_2(S_{left})$ and $\bar{S}_1 \leq \bar{S}_{left} \leq \bar{S}_1$ (Figs. 6 and 7) where \bar{S}_{left} is the

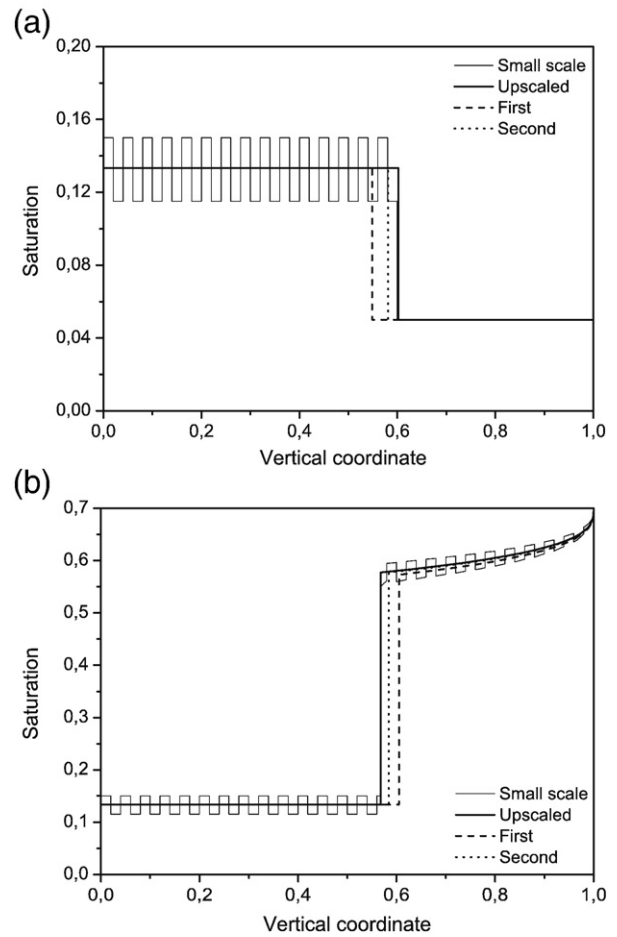


Fig. 10. Saturation distributions before (a) and after (b) the plume has reached the top of the column. Saturation at the bottom set to a value smaller than \bar{S}_1 . $k_-/k_+ = 0.3$.

saturation value, in the saturation range of the ascending rarefaction wave, at the vertical position of the reflected shock. $\bar{S}_{left} = \bar{S}_1$ when the plume reaches the top of the column and \bar{S}_{left} tends rapidly to \bar{S}_1 after that time. Again the “second order” reflected shock travels faster than the “first order” one. This is easily explained by the concave hulls of the first order and second order fluxes, not represented in Figs. 6

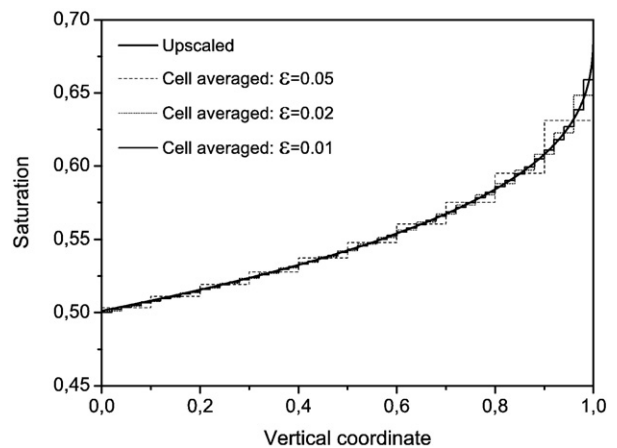


Fig. 11. Upscaled and cell averaged saturation distributions after the plume has reached the top of the column.

and 7. One can easily see that the slope of the straight line describing the reflected shock is greater for $k_-/k_+ = 0.05$ than for $k_-/k_+ = 0.3$.

For $k_-/k_+ = 0.3$, an additional simulation has been performed with a saturation fixed at the bottom of the column smaller than in the previous case, $\bar{S}(z = 0) = 0.14$. Indeed Figs. 6 and 7 show that, in the range $0 \leq \bar{S} \leq 0.14$, the discrepancies between the upscaled fluxes are smaller than in the previous range, $0 \leq \bar{S} \leq \bar{S}_1$, where $\bar{S}_1 = 0.21$. Fig. 10 displays the saturation distributions before and after the CO₂ plume has reached the top of the column. As expected, the plume front, described by a shock, is well approximated by the first and second order approximations, both before and after the plume reaches the top of the column. The second order provides an approximation of the plume transport better than the first order.

Finally, a convergence analysis with respect to ε has been performed. Fig. 11 shows the exact upscaled and cell averaged saturation profiles after the plume has reached the top of the column for $\varepsilon = 1/100$, $1/50$ and $1/20$. Convergence is clearly demonstrated.

4. Summary and conclusion

We have derived an upscaled model which describes the migration of a CO₂ plume in a vertical column filled with a periodic layered porous medium. Capillarity and buoyancy have been taken into account and two cases have been considered: (i) a capillary-dominant case where capillarity is the main driving force in a layer and (ii) a capillary-free case where buoyancy is the only driving force. The buoyant-dominant case, where buoyancy and capillarity are of the same order of magnitude in a layer, is much more complex and difficult to upscale. In the two cases, semi-explicit upscaled flux functions have been proposed. In both cases, the buoyant flux is a bell-shaped function of the saturation, as in the case of a homogeneous porous medium. In the capillary-dominant case, the upscaled saturation is governed by the continuity of the capillary pressure at the interface between layers. We showed that the upscaled buoyant flux is the harmonic mean of the buoyant fluxes in each layer, the high-permeability layer contribution being dominant. This result is unusual: low permeabilities usually control the harmonic mean. It is explained by the low value of the high-permeability layer buoyant flux. In the capillary-free case, the upscaled buoyant flux and upscaled saturation are determined by the flux continuity condition at the interface. As the flux is not continuous over the entire range of saturation, the upscaled saturation is only defined where continuity is verified: in low and high-saturation value domains. Therefore, the upscaled buoyant flux is described by a piecewise continuous function which has to be determined numerically. This is a direct consequence of the non-monotonicity of the buoyant flux function. We proposed two analytical approximations of the capillary-free upscaled flux. One of these approximations is simply the buoyant flux of a homogeneous layer with an effective permeability equal to the harmonic mean of the absolute permeabilities of the layers. The capillary-free model has been validated in two cases of heterogeneity by comparing small-scale and upscaled solutions obtained both theoretically. The upscaled saturation agrees well with the cell averaged saturation and the proposed analytical upscaled fluxes provide satisfactory approximations as long as the saturation set at the inlet of the column is in a range where analytical and numerical upscaled fluxes are close.

This upscaled model may describe the vertical migration of a CO₂ plume injected into a perfectly stratified aquifer far from the injection point where the plume lateral spreading may be neglected. It has been shown in this paper that injection can be taken into account in the upscaling procedure without difficulty, even if it leads to more intricate expressions of upscaled fluxes. The next step of this work will be to validate the capillary-dominant model with a numerical code and study the complex buoyant-dominant case.

Acknowledgments

This work has been supported by l'Agence Nationale pour la Recherche, programme capture et séquestration du CO₂ (National Agency for Research, CO₂ capture and sequestration program).

References

- [1] Aarnes J, Kippe V, Lie KA, Rustad AB. Modelling of multiscale structures in flow simulations for petroleum reservoirs. In: Hasle G, Lie KA, editors. Geometric modelling, numerical simulation, and optimization: Applied mathematics at SINTEF. Springer-Verlag; 2007.
- [2] Arts R, Eiken O, Chadwick A, Zweigel P, van der Meer L, Zinsner B. Monitoring of CO₂ injected at Sleipner using time-lapse seismic data. *Energy* 2004;29:1383–92.
- [3] Amaziane B, Bourgeat A, Koebe J. Numerical simulation and homogenization of two-phase flow in heterogeneous porous media. *Transport Porous Med* 1991;6: 519–47.
- [4] Ambrose WA, Lakshminarasimhan S, Holtz MH, Nunez-Lopez V, Hovorka SD, Duncan I. Geologic factors controlling CO₂ storage capacity and permanence: case studies based on experience, with heterogeneity in oil and gas reservoirs applied to CO₂ storage. *Environ Geol* 2008;54(8):1619–33.
- [5] Audigane P, Gaus I, Czernichowski-Lauriol I, Pruess K, Xu T. Two-dimensional reactive transport modelling of CO₂ injection in a saline aquifer at the Sleipner site, North sea. *Am J Sci* 2007;307:974–1008.
- [6] Bensoussan A, Lions JL, Papanicolaou G. Asymptotic analysis for periodic structures, studies in mathematics and its applications, vol. 5. Amsterdam, New York, Oxford: North-Holland; 1978.
- [7] Bickle M, Chadwick A, Huppert HE, Hallworth M, Lyle S. Modelling carbon dioxide accumulation at Sleipner: implications for underground carbon storage. *Earth Planet Sci Lett* 2007;255:164–76.
- [8] Birkholzer J, Tsang CF. Introduction to the special issue on site characterization for geological storage of CO₂. *Environ Geol* 2008;54(8):1579–81.
- [9] Brooks RH, Corey AT. Properties of porous media affecting fluid flow. *J Irrig Drain Div Am Soc Civ Eng* 1966;92(IR2):61–88.
- [10] Christie MA. Upscaling of reservoir simulation. *J Pet Technol* 1996:1004–10.
- [11] Christie MA, Blunt MJ. Tenth SPE comparative solution project: a comparison of upscaling techniques. *SPE J* 2001;4(4):308–17.
- [12] Cunha MCC, Santos MM, Bonet JE. Buckley–Leverett mathematical and numerical models describing vertical equilibrium process in porous media. *Int J Eng Sci* 2004;42(11–12):1289–303.
- [13] Dale M, Ekran S, Mykkeltveit J, Virnovsky G. Effective relative permeabilities and capillary pressure for one-dimensional heterogeneous media. *Transport Porous Med* 1997;26:229–60.
- [14] Doughty C, Pruess K. Modeling supercritical carbon dioxide injection in heterogeneous porous media. *Vadose Zone J* 2004;837–47.
- [15] Doughty C. Modeling geologic storage of carbon dioxide: comparison of non-hysteretic and hysteretic characteristic curves. *Energy Convers Manage* 2007;48: 1768–81.
- [16] Flett M, Gurton R, Weir G. Heterogeneous saline formations for carbon dioxide disposal: impact of varying heterogeneity on containment and trapping. *J Pet Sci Eng* 2007;57(12):106–18.
- [17] Green CP, Ennis-King J. Effect of vertical heterogeneity on long term migration of CO₂ in saline formations. *Transport Porous Med* 2010;82:31–47.
- [18] Hayek M, Mouche E, Mügler C. Modeling vertical stratification of CO₂ injected into a deep layered aquifer. *Adv Water Resour* 2009;32:450–62.
- [19] Hesse MA, Woods AW. Buoyant dispersal of CO₂ during geological storage. *Geophys Res Lett* 2010;37:L01403.
- [20] Johnson JW, Nitao JJ, Knauss KG. Reactive transport modelling of CO₂ storage in saline aquifers to elucidate fundamental processes, trapping mechanisms and sequestration partitioning. In: Baines SJ, Worden RH, editors. Geological Storage of Carbon Dioxide, 233. Geological Society of London Special Publications; 2004. p. 107–28.
- [21] Kaasschieter EF. Solving the Buckley–Leverett equation with gravity in a heterogeneous porous medium. *Comput Geosci* 1999;3:23–48.
- [22] Kumar A, Ozah O, Noh M, Pope GA, Bryant S, Sepelinoori K, Lake LW. Reservoir simulation of CO₂ storage in deep saline aquifers. *SPE J* 2005:336–48.
- [23] Lewandowska J, Szymkiewicz A, Burzynski K, Vauclin M. Modeling of unsaturated water flow in double-porosity soils by the homogenization approach. *Adv Water Resour* 2004;27:283–96.
- [24] Leverett MC. Capillary behavior in porous solids. *Trans AIME Petr Eng Div* 1941;142:152–69.
- [25] Neufeld JA, Huppert HE. Modelling carbon dioxide sequestration in layered strata. *J Fluid Mech* 2009;625:353–70.
- [26] Panfilov M, Floriat S. Nonlinear two-phase mixing in heterogeneous porous media. *Transport Porous Med* 2004;57:347–75.
- [27] Pickup G, Ringrose PS, Sharif A. Steady-state upscaling: from lamina scale to full field model. *SPE J* 2000;5(2):208–17.
- [28] Quintard M, Whitaker S. Two-phase flow in heterogeneous porous media: the method of large-scale averaging. *Transport Porous Med* 1988;3:357–413.
- [29] Quintard M, Whitaker S. Two-phase flow in heterogeneous porous media II: numerical experiments for flow perpendicular to a stratified system. *Transport Porous Med* 1990;5:429–72.
- [30] Renard P, de Marsily G. Calculating equivalent permeability: a review. *Adv Water Resour* 1997;20:253–78.

- [31] Ringrose PS, Martinius AW, Alvestad J. Multiscale geological reservoir modelling in practice. *Geol Soc Lond Spec Publ* 2008;309:123–4.
- [32] Saadatpoor E, Bryant SL, Sepehrnoori K. New trapping mechanism in carbon sequestration. *Transport Porous Med* 2010;82:3–17.
- [33] Sanchez Palencia E. Non-homogeneous media and vibration theory. *Lectures Notes in Physics*, 127. Berlin: Springer-Verlag; 1980.
- [34] Siddiqui FI, Lake LW. A dynamic theory of hydrocarbon migration. *Math Geol* 1992;24:305–27.
- [35] Siddiqui FI, Lake LW. A comprehensive dynamic theory of hydrocarbon migration and trapping. *SPE* 1997;395–410.
- [36] Sillin D, Patzek T, Benson SM. A model of buoyancy-driven two-phase countercurrent fluid flow. *Transport Porous Med* 2009;76:449–69.
- [37] Torp TA, Gale J. Demonstrating storage of CO₂ in geological reservoir: the Sleipner and SACS project. GHGT-7 conference proceeding Greenhouse Gas Control Technologies; 2002.
- [38] van Duijn CJ, Molenaar J, de Neef MF. The effect of capillary forces on immiscible two-phase flow in heterogeneous porous media. *Transport Porous Med* 1995;21:71–93.
- [39] van Duijn CJ, de Neef MF. Similarity solution for capillary redistribution of two phases in a porous medium with a single discontinuity. *Adv Water Resour* 1998;21:451–61.
- [40] van Duijn CJ, Mikelić A, Pop IS. Effective equations for two-phase flow with trapping on the micro scale. *SIAM J Appl Math* 2002;62:1531–68.
- [41] van Duijn CJ, Eichel H, Helmig R, Pop IS. Effective equations for two-phase flow in porous media: the effect of trapping on the microscale. *Transport Porous Med* 2007;69:411–28.
- [42] van Genuchten MTh. A closed-form equation for predicting the hydraulic conductivity of unsaturated soils. *Soil Sci Soc Am J* 1980;44:892–8.